Research paper

Identifying the scale-dependent motifs in atmospheric surface layer by ordinal pattern analysis

Qinglei Li [a,b], Zuntao Fu [b,*]

[a] National Meteorological Information Center, Beijing, 100081, China
[b] Lab for Climate and Ocean-Atmosphere Studies, Department of Atmospheric and Oceanic Sciences, School of Physics, Peking University, Beijing 100871, China

A B S T R A C T

Ramp-like structures in various atmospheric surface layer time series have been long studied, but the presence of motifs with the finer scale embedded within larger scale ramp-like structures has largely been overlooked in the reported literature. Here a novel, objective and well-adapted methodology, the ordinal pattern analysis, is adopted to study the finer-scaled motifs in atmospheric boundary-layer (ABL) time series. The studies show that the motifs represented by different ordinal patterns take clustering properties and 6 dominated motifs out of the whole 24 motifs account for about 45% of the time series under particular scales, which indicates the higher contribution of motifs with the finer scale to the series. Further studies indicate that motif statistics are similar for both stable conditions and unstable conditions at larger scales, but large discrepancies are found at smaller scales, and the frequencies of motifs "1234" and/or "4321" are a bit higher under stable conditions than unstable conditions. Under stable conditions, there are great changes for the occurrence frequencies of motifs "1234" and "4321", where the occurrence frequencies of motif "1234" decrease from nearly 24% to 4.5% with the scale factor increasing, and the occurrence frequencies of motif "4321" change nonlinearly with the scale increasing. These great differences of dominated motifs change with scale can be taken as an indicator to quantify the flow structure changes under different stability conditions, and motif entropy can be defined just by ***only 6 dominated motifs*** to quantify this time-scale independent property of the motifs. All these results suggest that the defined scale of motifs with the finer scale should be carefully taken into consideration in the interpretation of turbulence coherent structures.

© 2018 Elsevier B.V. All rights reserved.

1. Introduction

Simple visual inspections of different kinds of atmosphere boundary layer (ABL) time series reveal that marked structures appear on multiple time scales, from the smallest turbulence scales up to several days [1]. That's because there are many different physical processes with abrupt nature over a broad range of scales in the atmosphere, which force, modify and coexist with the ABL turbulence [2–4]. One of the well-studied marked structures in various ABL time series is the ramp-like structures, in which a slow, nearly steady increase or decrease is followed by a relatively rapid change back to a base-line

---

level [5–7]. They are ubiquitous at varied scales in series (i.e., smaller ramps and spikes are embedded in larger ramps), and significantly contribute to the forming of flow properties [8], such as generation of smaller scale turbulence and transport of scalars [1,4]. However, the presence of motifs with the finer scale, which are embedded within larger scale ramp-like structures, has largely been overlooked in the reported literature, although they can readily be perceived in turbulent traces [9]. What's more, relatively large uncertainties have been reported in the determinations of ramp-like structure duration and separation times in various ABL series [8].

Ramp-like structures in various atmospheric surface layer time series have been long studied by scientists using different techniques [8,10], which indicates that identifying ramp-like coherent structures in the surface layer is still a challenge task. Taylor [10] was the first one to observe and comment on the ramp features in a study of temperature at several heights in the atmospheric boundary layer. Since Taylor's seminal work, ramp-like coherent structures have been studied and detected in time series through different conditional sampling techniques, such as intermittency function [11], variable interval time average [12–14], multi-level detection scheme [15], quadrant analysis [16,17], and wavelet transform [18–23]. Collineau [18] used wavelet transform to extract information on turbulence structure from time series of wind velocities and scalars for various applications. Hagelberg [19] illustrated the dependence of the coherent structure detection mechanism on the choice of analyzing wavelet, demonstrating that particular anti-symmetric wavelets are better suited to detecting zones of concentrated shear. The wavelet transform has also been used to detect the time scales of coherent structures [20] and to study their effects on the dynamics of turbulent transport processes [21,22]. The structure function with varied time lags provide another possibility for identifying the characteristic duration and amplitude of the ramps [8,24–27]. Using structure function analysis, Calif and Schmitt [27] showed that the atmospheric wind speed and the aggregated power output from a wind farm are intermittent and multi-fractal over a wide range of scales. However, there is considerable disagreement among these results concerning the definition of the ramp-like structures' boundaries. Yuan and Mokhtar [28] applied several conditional sampling methods to wind tunnel turbulent data and arrived at the conclusion that no two methods detect exactly the same event ensemble, and some methods even detect different parts of the same event sometimes. Especially, it should be pointed out that many ramp identification procedures are evaluated mainly by subjective thresholds and visual inspection of the time series [28], but this may overlook motifs of finer scale that are not readily identified due to these methods' limitations [8].

The limitations of the above mentioned methods are due to their dependence on the selection criteria, as for wavelet analysis, its processing is computational time consuming [20,23] and even impossible since the chosen wavelet shapes are different from the turbulent ramp structures [8]. Therefore, some objective and well-adapted techniques should be used to overcome these limitations in order to better characterize and understand the scale-dependent structures. The recent development of nonlinear methods in time series analysis makes it possible to reveal new discoveries. The ordinal pattern analysis [29] is such kind of methods that has been widely used in various fields of science [30–35], such as global climate change [31,32], vertical wind velocity [35] and so on. One of benefits of this method is its invariance with respect to nonlinear monotonous transformations [29]. It is simply based on comparing values in the time-series to construct "ordinal patterns", which represent different motifs of the scale-dependent structures in time series. Using multi-scaled ordinal pattern analysis, no restriction is made on particular time scales, unlike that in the structure function analysis for a ramp model with two scales, which respectively represent the smaller size non-flux-bearing turbulence and the larger the main flux-bearing eddies [8]. Recently, various nonlinear time series models have also found a widespread application in many practical sciences [36–52] successfully, such as monthly rainfall forecast in water resources management [47], optimization of irrigation efficiency in agricultural [48,49], and evapotranspiration computation under different weather or climate conditions [50–52], just list some among them [36–52]. Herein, based on the symbolic nonlinear time series method, the time-scale dependent property of motifs will be well studied within the research of the atmospheric surface-layer turbulence.

The purpose of this study is: (1) to identify and more importantly quantify the dependence of motifs with the finer scale in surface-layer vertical wind fluctuations on time scale and stratification stability; (2) to adopt a novel, objective and well-adapted methodology, the ordinal pattern analysis, to study of motifs with the finer scales in ABL research. The key contributions of this paper are: (1) for the first time, the symbolic nonlinear time series method based on comparing neighbor values is used to identify and quantify the scale-dependent motifs in atmospheric surface layer; (2) the studies indicate that motif statistics are similar for both stable conditions and unstable conditions at larger scales, but large discrepancies are found at smaller scales, and the frequencies of motifs "1234" and/or "4321" are a bit higher under stable conditions than unstable conditions; (3) measures from ***only some dominated motifs*** can present the flow changes of the whole series; (4) a detailed and better understanding of the surface-layer turbulence structure will be beneficial to simulate physical processes of boundary layer in numerical model, such as air pollution diffusion processes and wind power prediction.

2. Data and methods

2.1. Data

Atmospheric boundary-layer turbulence records used here are collected during the field experiment in Huaihe River Basin from 9 to 22 June 1998. The observation site is located on the western edge of a large paddy field. A three-dimensional sonic anemometer (SAT-211/3 K, sampling rate 10 Hz, located 4 m above ground) has been used to measure wind velocity components and temperature, and more detailed information can be found in the reported literatures [20,35,53–56]. This

Table 1
Notations used through the proposed methodology.

$\langle \boldsymbol{x} \rangle$	the time averaging of a measured variable x
$\boldsymbol{x'}$	the deviation from the mean of a measured variable x
$\boldsymbol{\pi}$	the permutation
#	the number (frequency) occurrences of the permutation π
$\boldsymbol{P}$	the permutation probability distribution
$\boldsymbol{PE_s}$	the permutation entropy
$\boldsymbol{ME_{s1}}$	the motif entropy for 6 dominated motifs
$\boldsymbol{ME_{s2}}$	the motif entropy for residual 18 motifs

data set has been widely studied to analyze the characteristics of turbulence in the ABL, and some nonlinear features have been derived [54–56].

In order to differentiate the flow changes in the ABL, two broad stratification stability categories are considered herein: unstable stratification conditions ($z/L < -0.1$) and stable stratification conditions ($z/L > 0.1$), where $z = z_m - d$, z_m is the measurement height, d is the displacement height and $L = -u_*^3 \langle T \rangle / \kappa g \langle w'T' \rangle$ is the Obukhov length [57], where $u_* = [\langle u'w' \rangle^2 + \langle v'w' \rangle^2]^{1/4}$ is the friction velocity, T is temperature, $\kappa (= 0.4)$ is the von Karman constant, and g is the acceleration due to gravity. There are 24 vertical velocity time series selected for research where each has 40,000 sampling points, and 12 of them are under unstable stratification conditions while the other 12 are under unstable stratification conditions. We show the ensemble-averaged statistical results with its unit standard deviation as error bars from 12 samples for each group.

Herein the authors mainly focus on the vertical components of wind velocity w and the method is suitable for latitude and longitude wind velocity (u and v), since there is sufficient evidence indicating that the vertical wind shear is the major factor in the generation of coherent structures in the surface layer [5,58,59].

2.2. Methods

It is very convenient to represent time series symbolically by means of ordinal patterns, which is carried out by comparing neighboring values of the original series [30] and one can numerically break equalities by adding small random perturbations if some equal neighboring values exist in series [60], since equalities in the input signal can lead to false conclusions in the studies [61].

For a given series $\{x_t\}_{t=1,2,...N}$ and an embedding dimension $D > 1$, the ordinal pattern of order D is given by

$$(s) = \left(x_{s-(D-1)}, x_{s-(D-2)}, \ldots x_{s-1}, x_s \right) \tag{1}$$

with $s = D, \ D + 1, \ldots, N$.

The permutation $\pi = (r_0, r_1, \ldots, r_{D-1})$ for each of these $(N - D + 1)$ vectors of $(0, 1, \ldots, D - 1)$ is defined by

$$x_{s-r_{D-1}} \leq x_{s-r_{D-2}} \leq \ldots \leq x_{s-r_1} \leq x_{s-r_0} \tag{2}$$

For all D! possible permutations of π, the probability distribution $p(\pi)$ is given by

$$p(\pi) = \frac{\#\{s \mid s \leq N - D + 1; \ (s) \text{has type } \pi\}}{N - D + 1} \tag{3}$$

with the symbol # stands for the occurrence frequency of the permutation π. Notations used in this paper are summarized in Table 1.
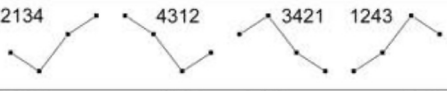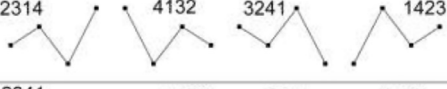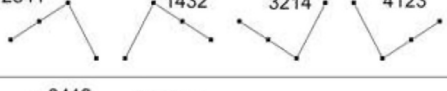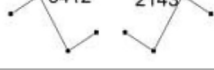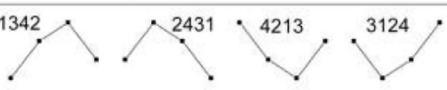
In fact, the constraint $D! \ll N$ must be fulfilled to obtain a reliable statistics, so Bandt and Pompe recommended $D = 3, \ 4, \ldots, 7$ for practical purposes [60] and in this paper $D = 4$ has been fixed (Actually, the value of D, say 3 or 5, will not change the conclusions given in this paper, figures are not shown here). Table 2 depicts all 24 ordinal patterns (24 different motifs) of length $D = 4$ gathered in groups, and the number after each motif in the end of the line denotes ordinal pattern index used in Figs. 3 and 4. What's more, examples of motif "4123" are showed in Fig. 1(g).

It should be noted that ramp-like structures are closely related to the particular motif occurrence frequency, such as "1234" and "4321", since the mean of the series stays nearly unchanged. The high occurrence frequencies of "1234" and other patterns with increasing trend indicate in principle that the motifs with a gradual rise followed by a sudden fall cover a great part in the series, while the inverted motifs with a gradual fall followed by a sudden rise account for a comparatively great proportion if the motif "4321" and other motifs with decreasing trend occur more frequently.

In order to identify the dependence of motifs on time scales and to quantify the multi-scale features in the atmospheric turbulent motions, the time series are suitably block averaged [1] under different time windows: $T_s = 2^h$ with the scale factor $h = 0, 1, \ldots, 9$. This procedure is very different from the authors' previous reported work [35], in which the scale factor is used on the first order structure function, indicating vertical wind velocity increments under different time lags (the lag or time delay method [62,63] can also work well in this direction as block average, similar results will be reached quantitatively). Herein it physically corresponds to multiples of the sampling time of the given time series, in order to show the scale-dependent properties of different motifs. Therefore, the sampling rate of 10 Hz enables the minimum ordinal

Table 2
Motifs of length $D = 4$ gathered in groups, the number after each motif in the last line denotes pattern index used in Fig. 3. Particularly, the motifs in bold font are mainly discussed here for better understanding.

pattern time scale of 0.4 s, with the subsequent scales distributed as follows: 0.8 s, 1.6 s, 3.2 s, 6.4 s, 12.8 s, 25.6 s, 51.2 s, as shown in Fig. 1.

The scale-dependent statistical properties of ordinal patterns can be captured by the permutation entropy [60], which is the normalized entropy of the probabilities of different ordinal patterns,

$$PE_s[P] = \frac{-\sum_{\pi=1}^{D!} p(\pi)\log[p(\pi)]}{\log D!} \tag{4}$$

Naturally, $0 \leq PE_s[P] \leq 1$, where the upper bound $PE_s[P] = 1$ occurs for a completely random process, in which all D! possible permutations are equal-probable. $PE_s[P]$ will be smaller than one if the time series exhibits some kind of ordering dynamics. The parameter D determines the number of accessible motifs, which plays an important role in the estimation of the permutation probability distribution P and the corresponding permutation entropy $PE_s[P]$ [64].

Since 6 dominated motifs out of the whole D! = 24 motifs show marked time-dependent properties than others (see Fig. 3 and Fig. 4.), herein we introduce motif entropy (*ME*) to quantify these differences. Comparing with *PE*, the ME_{s1} only takes 6 dominated motifs into consideration and ME_{s2} the residual 18 motifs,

$$\begin{cases} ME_{s1}[P] = \dfrac{-\sum_{\pi=1,2,7,18,23,24} p(\pi)\log[p(\pi)]}{\log D!} \\[4mm] ME_{s2}[P] = \dfrac{-\sum_{\pi \neq 1,2,7,18,23,24} p(\pi)\log[p(\pi)]}{\log D!} \end{cases} \tag{5}$$

where $\pi = 1, 2, 7, 18, 23, 24$ is the 6 dominated ordinal pattern index in Table 2. Similarly, $0 \leq ME_{s1}[P] + ME_{s2}[P] \leq 1$, where the theoretical bound $ME_{s1}[P] = 0.25$ and $ME_{s2}[P] = 0.75$ occur for a completely random process with all 24 possible motifs are equal-probable.
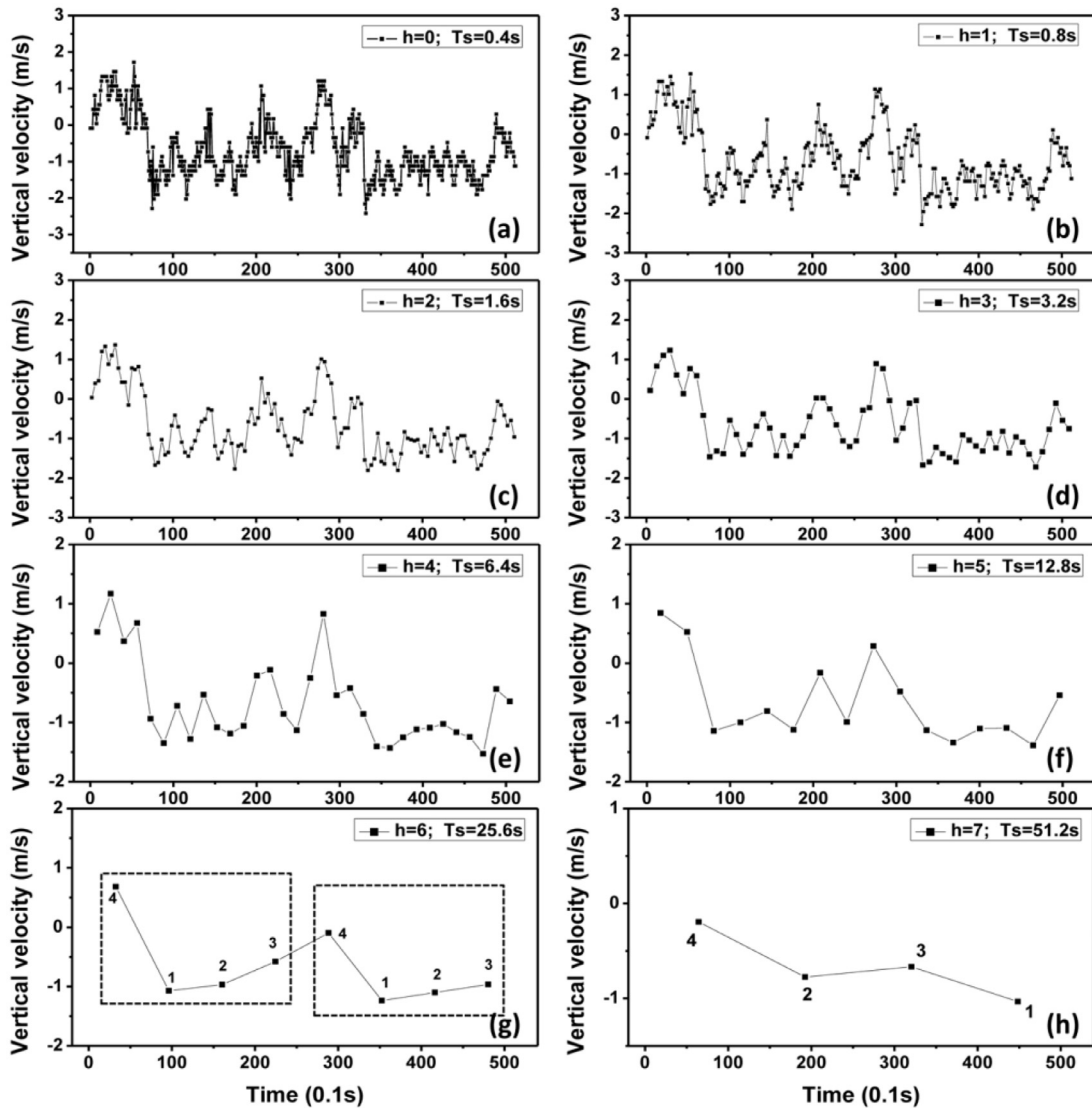
Fig. 1. The time series of vertical velocity with motifs under different scale factors: (a) $h = 0$, $T_s = 0.4$ s; (b) $h = 1$, $T_s = 0.8$ s; (c) $h = 2$, $T_s = 1.6$ s; (d) $h = 3$, $T_s = 3.2$ s; (e) $h = 4$, $T_s = 6.4$ s; (f) $h = 5$, $T_s = 12.8$ s; (g) $h = 6$, $T_s = 25.6$ s; (h) $h = 7$, $T_s = 51.2$ s; Examples of motif "4123" and "4231" are showed in Fig. 1(g) and Fig. 1(h).

3. Results

3.1. Ordinal patterns under different time scales

Fig. 1 shows ordinal patterns under different time scales. When the scale factor is smaller (the block window is smaller), the symbolized series will still preserve the basic feature from the original measurements, see Fig. 1(a) and (b). However with the block window increasing, most of detailed large fluctuations will be smoothed off and the large scale structures will be weakened, see Fig. 1(e) and (f). At last, larger scale effects from the dominated motifs are eliminated since the ever changing occurrence frequencies of different motifs are nearly unchanged at scales larger than 51.2 s, see Fig. 1(h). Consequently, different time scales smaller than 1 minute are considered by changing the scale factor of the symbolic reconstructions. One of the marked features here in these time series is the emergence of ramp-like structures, such as, a rapid decrease is followed by a relatively slow change back to a base-line level, see motif "4123" in Fig. 1(g). The changes in frequencies of different ramp-like structures are not homogeneous, however, they change gradually with time scales.

Simple visual inspections of vertical wind velocity series reveal that motifs appear on a large range of time scales. Fig. 2 shows the randomly chosen examples on two different scales. Both vertical wind velocity series possess 30 ordinal patterns
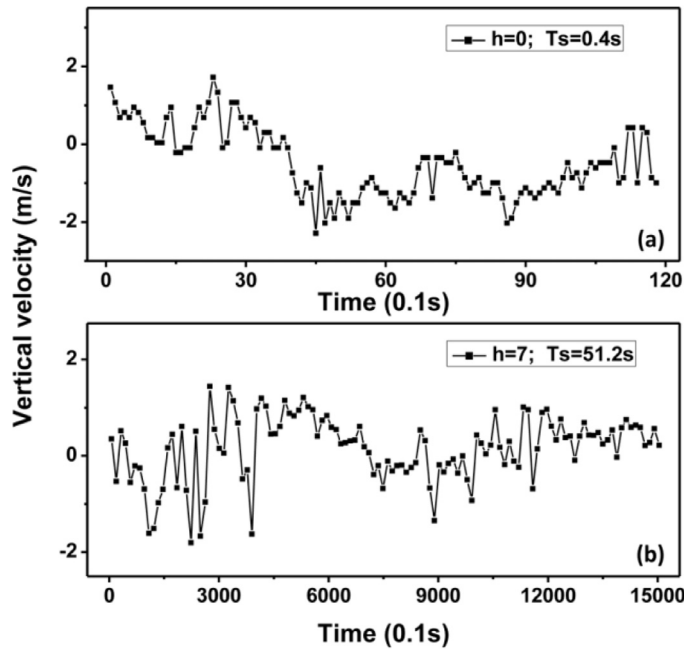
Fig. 2. For visual identification, vertical velocity time series segments under different scale factors, but with equal number of data points or motifs: (a) $h = 0$, $T_s = 0.4$ s; (b) $h = 7$, $T_s = 51.2$ s.

($D = 4$) measured at the same location, but on two different time scales. Though particular motifs account for a greater proportion at smaller time scales in Fig. 2(a), an untrained eye cannot distinguish between the motifs on different scales.

3.2. Occurrences of ordinal patterns

In order to better characterize the difference, the occurrence frequency of all 24 motifs with $D = 4$ is calculated under different time scales, see Fig. 3. First of all, it reveals a clustered organization of the probabilities: motifs "1234" and "4321" occur with nearly similar probability, while motifs "1243", "2134", "3421" and "4312" have the similar occurrence frequency, and so on. Secondly, the probabilities of the same group of motifs present the same revolution with changing time scale.

At the lower level of block window (such as the original measurements $h = 0$ or $h = 1$), there are marked different behaviors in vertical wind velocity series between the stable and unstable stratifications, the occurrence frequency of motifs "1234" and "4321" is symmetric on the unstable stratification, but asymmetric on the stable stratification with larger amount (16%) of motif "1234" and smaller amount (8%) of motif "4321", see Fig. 3(a). As the block window increases, the observed difference between the stable and unstable stratifications will be weakened, just like what is shown in Fig. 3(b), with scale factor $h = 2$, the occurrence frequency of motifs "1234" and "4321" is all nearly 12%, while the value is 6% for motifs "1243", "2134", "3421" and "4312", and all the above 6 motifs out of the whole 24 motifs account for about 45% of the time series. However, the occurrence frequency of motifs "2413" and "3142" is smaller than 2%, which are the smallest ones. The occurrence frequency of motifs "1234", "1243", "2134", "3421", "4312" and "4321" are much higher than others under smaller scale factors (see, $h = 1, 2, 3$), which is an indicator that the following two kinds of motifs are in majority[23]: (i) a gradual rise is followed by a sudden fall or (ii) the pattern is inverted and a sudden rise is followed by a gradual fall. It has been recognized that such kind of downdrafts (or sweeps) and updrafts (or ejections) are the primary constitutive motions of such ramp-like patterns in planetary boundary-layer turbulence [65].

With the scale factor increasing, the occurrence frequencies of different motifs gradually change, see Fig. 3(c)–(f). With the scales increasing, the motifs with higher occurrence frequencies at scale $h = 1$ become less, the others occur more. When the scale factor reaches $h = 7$ as shown in Fig. 3(f), the occurrence frequency is nearly the same for all 24 motifs, which is 4.17% as found in white noise series without any preferred motif at any scales. It has also been found that steep edges of shapes weakens with increasing scale [1], which seems to be predominantly related to downward transport of heat and momentum. Here our results are consistent with these previous studies [23,35,65].

At larger scales (see $h = 7$), the above results are similar for both stable conditions and unstable conditions. However, large discrepancies are found at smaller scales (see $h = 3, 4$), and the frequencies of motifs "1234" and "4321" are a bit higher under stable conditions than under unstable conditions. It means that the sweeps and ejections are much common in stable conditions. Our results coincide with the conclusion that coherent structures occur more often under stable conditions than for unstable conditions but with smaller length scales [23]. The stability dependence of the motif frequency or the coherent structure duration times emphasize the role of stratification on the formation of coherent eddies.
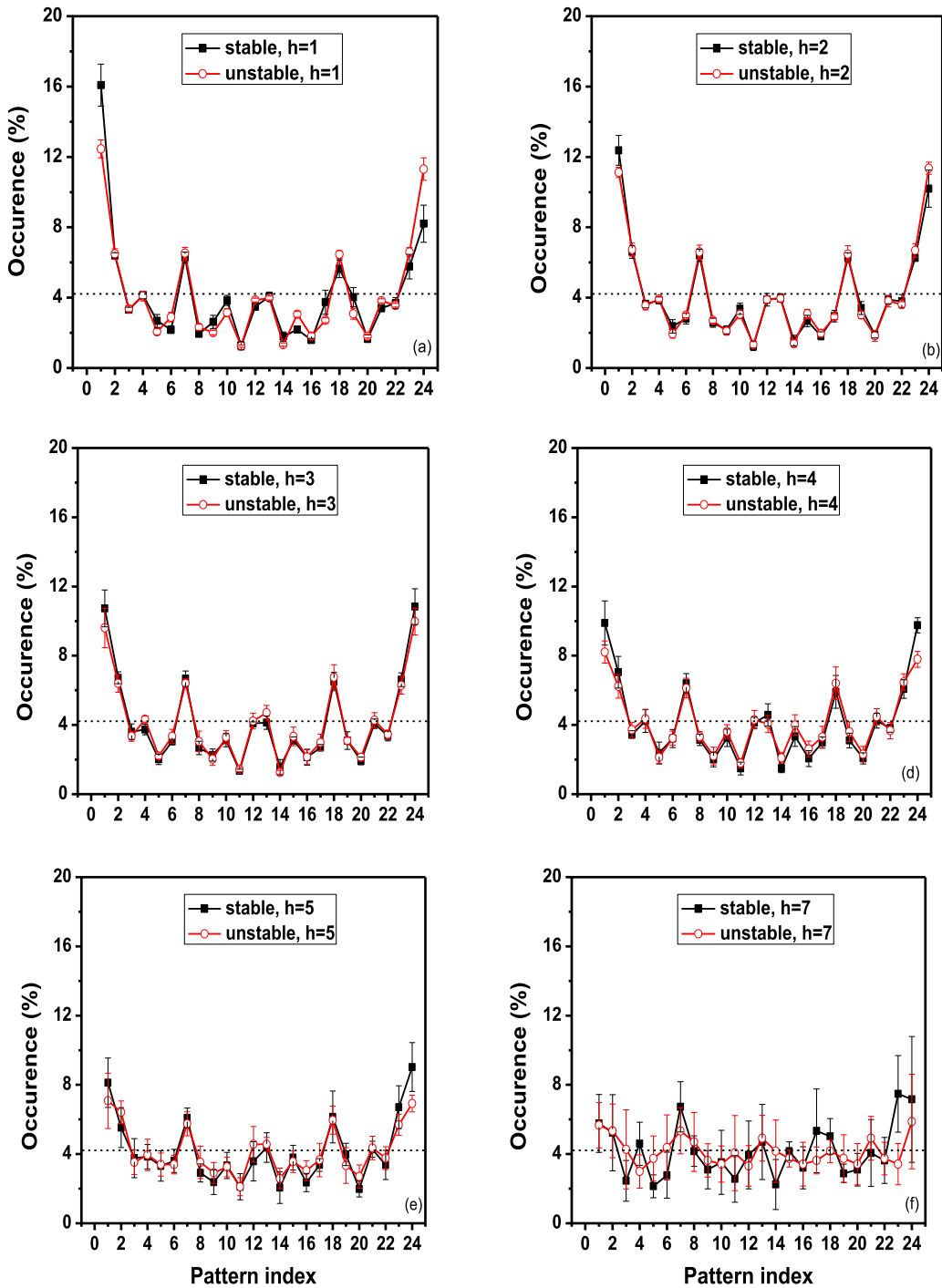
Fig. 3. The occurrence frequency of 24 motifs under different scale factors: (a) $h = 1$; (b) $h = 2$; (c) $h = 3$; (d) $h = 4$; (e) $h = 5$; (f) $h = 7$; the dash line denotes the averaged frequency 4.17% for each motif.

Fig. 4 shows the changing occurrence frequency of typical motifs with varied scale factor h in vertical velocity time series under stable stratification condition (Fig. 4(a)) and unstable stratification condition (Fig. 4(b)). For both stable and unstable conditions, first of all, it can be seen that at the same scale factor, the motifs show clustering properties as shown in Fig. 3. Secondly, with the scale increasing, the frequencies of all motifs tend toward a stable value around 4.17% as in white noise series. Thirdly, the time scale at which the frequencies of different motifs converge to their constant values is about $h = 7$, $T_s = 51.2$ s. At last and most importantly, there are great changes for the occurrence frequencies of motifs "1234"
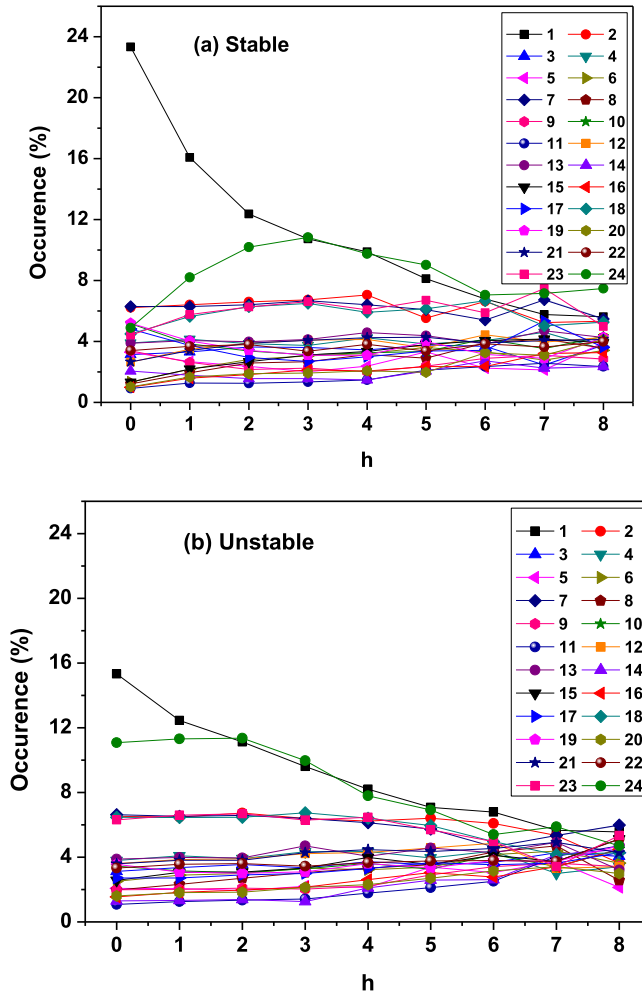
Fig. 4. The changing occurrence frequency of typical motifs in vertical velocity time series with different scale factor *h*. (a) under stable conditions, (b) under unstable conditions.

and "4321". The occurrence frequencies of motif "1234" decrease from nearly 24% to 4.5% under stable conditions with the scale factor increasing, while nearly 16% to 5% under unstable conditions. The occurrence frequencies of motif "4321" change nonlinearly with the increasing scale factor under stable conditions, while nearly unchanged at smaller scales ($h \leq 2$), and decrease linearly at larger scales under unstable conditions. These great differences of these dominated motifs between stable and unstable conditions can be taken to define a new indicator to differentiate and quantify the flow changes under different conditions.

3.3. Entropy analysis and quantification of organization degree

The above differences between varied time scales and the changing occurrence frequencies of different motifs are more descriptive or qualitative, in order to deeply understand their dependency on time scales, more quantitative results are required. Shannon entropy (*SE*) has been used to quantify the organization of atmospheric turbulent eddy motion by Wesson et al. [57]. What is more, *PE* provides other parameters similar to *SE* that can quantify the organization degree of a given time series [29] and can efficiently identify the characteristic time scales of the relevant physical system [35,66].

The results shown in Fig. 4 indicate that the great changes of motif occurrence with scales only happen for some dominated ones, and these suggest that quantifying the organization of atmospheric turbulent eddy motion may not require all the patterns just as *SE* or *PE*. Applying the motif entropy (*ME*) defined in Eq. (5), the flow features under different stability conditions are quantitatively shown in Fig. 5(a), where **only 6 dominated motifs** have been included in the calculations of ME_{s1}. Indeed, marked differences can be found between stable and unstable conditions. At the same time, the prominent feature for both cases is that the behavior of ME_{s1} is nearly symmetrical about a horizontal line to that of ME_{s2}. Firstly, with scale factor increasing, both ME_{s1} and ME_{s2} tend to their saturation levels, but at larger scales ($h \geq 2$), the vertical wind ve-
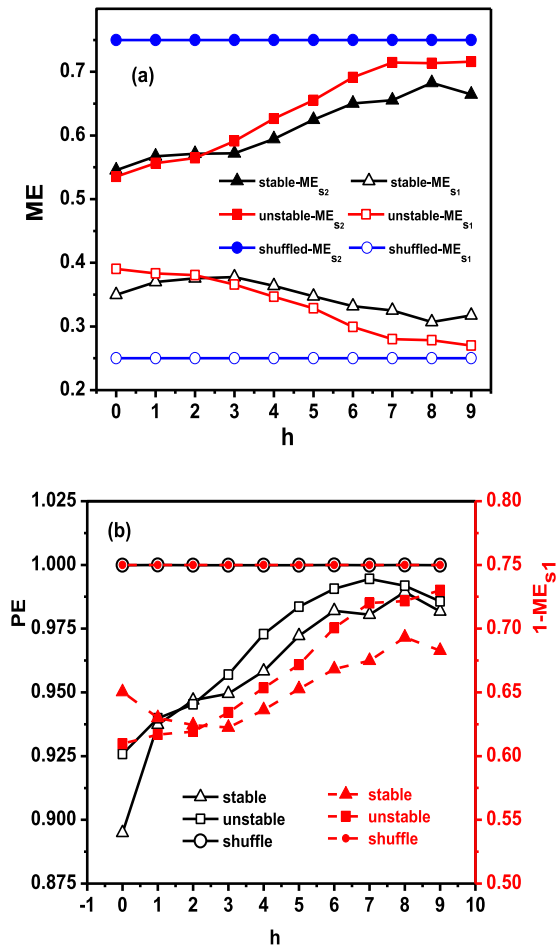
Fig. 5. The permutation entropy changing with time scale for vertical velocity series under stable and unstable conditions, as well as the shuffled time series. (a) the motif entropy, (b) Comparison between PE_s and $1 - ME_{s1}$.

locities under unstable condition are much closer to the homogenous states, where the occurrence frequency of each motif is equal. Secondly, ME_{s1} and ME_{s2} under unstable conditions will reach their saturation levels on much smaller scale, such as $h = 7$, but for stable conditions, they still do not reach the saturation levels when $h = 9$. This indicates that the heterogeneity is much heavier (the difference among the occurrence frequencies of 6 chosen motifs are much larger) for vertical velocity under stable conditions, especially at smaller scales $h < 2$, which is related to the heavier turbulence intermittency. These results of ME_{s1} of 6 dominated motifs can help to catch most of details on the scale-dependent properties.

From the definitions given in Eqs. (4) and (5), we know that $PE_s[P] = ME_{s1}[P] + ME_{s2}[P]$. Since there are nearly symmetrical behaviors between ME_{s1} and ME_{s2} under both stable and unstable conditions, we can expect that the results of $1 - ME_{s1}[P]$ of 6 dominated motifs will catch most of PE_s scale-dependent behaviors. Comparison between $1 - ME_{s1}[P]$ behaviors and PE_s behaviors (see Fig. 5(b)) indicates this conjecture is nearly totally correct except stable cases over smaller scales ($h < 2$). Independent on the stratification stability, the values of PE_s are all lower at $h = 0$ for the original time series than that at $h = 1$ for the block averaged time series with time windows $T_s = 0.4\,\text{s}$, where no signature of the noise in the recording time series has been found, as shown in the theoretical and numerical simulations [67]. For $1 - ME_{s1}[P]$, the unstable cases can recover these behaviors very well, however, the results for stable cases are totally different, which is from the dominated occurrence frequency of motifs "1234" at $h = 0$ and $h = 1$ (see Fig. 4(a)). Secondly, the scales at which the both entropies reach its maximum are nearly the same for both stable and unstable conditions, in accordance with the reported results that the duration and separation times of the structures are highly variable in the surface layer but the dominant separation times do not depend on atmospheric stratification [23]. Thirdly, both $1 - ME_{s1}[P]$ and PE_s increase with scale factor for both stable and unstable conditions when $h > 2$, and they are all smaller for stable conditions than that under unstable conditions, which is an indicator that coherent structures occur more frequently under stable conditions than under unstable conditions but this difference is dominated with smaller length scales [23].

Both changing entropies ME_{s1} and PE_s with scales indicates that the motifs are multi-scaled as shown in Fig. 3, such that motifs and spikes with the finer scale are embedded in larger motifs (or ramps[9]). Under different time scales, the motifs

account for different proportions, since the occurrence frequency of motifs "1234" and "4321" change most significantly. The motif entropy from only limited motifs can work well in quantifying the organization degree of the motifs under different scales. At a particular scale, the time series is more close to the behavior of white noise if it possesses smaller ME_{s1}; while the series is much well organized and the greater the proportion of motifs if the ME_{s1} gets larger. Shapland et al. [8] have proposed that smaller scale ramps and ramp-like spikes are the signature of non-flux-bearing turbulence, and resolving the characteristic of these shapes will shed light on small-scale turbulent processes. On the other hand, Shapland et al. [8] have also proposed that the characteristics of larger scale ramps provide information on flux-bearing coherent structures. Herein the scale ($h = 6, 7$) at which the ME_{s1} nearly reaches its saturation is about 30~50 seconds, which is consistent with the previous wavelet analysis results which indicates that the wavelet energy has local maximum values at time scales about 30 s, corresponding to the scales or frequencies of typical coherent structures [20].

4. Discussions

The atmospheric winds exhibit variations on multiple time scales, in principle ranging from seconds (and less) up to centuries. One of the consequences of multiple scales is that small scale fluctuations are strongly non-Gaussian and characterized by 'spiky' behavior (turbulence intermittency). The challenge is that traditional methods like power spectrum analysis are susceptible to these nonlinear variations which are commonly encountered [56,68]. Small-scale intermittency is still taken as a challenging problem for the turbulence community research [69,70], though many different methods have been used to characterize it. For example, structure function provides a method for determining the turbulent ramp characteristics and the turbulence intermittency [8,26,71]. The probability density functions (PDFs) of multi-scaled velocity increments show a transition from Gaussian distributions to intermittent (heavy-tailed) ones as scale decreases, and large increment values in the tails directly correspond to an increased probability to observe large events, such as wind gusts [56,72–74]. Better characterizing small-scale wind fluctuations is important for many applications, for example, the wind variations have a very significant effect on the design and performance of the individual wind turbine [73], on scales down to several seconds.

Herein, the authors adopted a novel expression, which is based on ordinal pattern and permutation entropy, to better characterize the scale-dependent properties of motifs in wind fluctuations. Studies show that motifs with the finer scales show clustering properties, and 6 dominated motifs out of the whole 24 motifs account for more than 45% of the time series on some particular scales. And results are similar for both stable conditions and unstable conditions at larger scales, but large discrepancies are found at smaller scales (see $h = 0, 1$), and the frequencies of motifs "1234" and "4321" are a bit higher under stable conditions than under unstable conditions, which is consistent with previous study [23]. Motif entropy analysis based on ***only limited ordinal patterns (here only 6 dominated motifs are considered)*** can be an efficient method to quantify the organized features of the motifs with different scales in surface-layer wind speed time series.

The results show that at smaller scales the following two kinds of motifs are in majority [23]: (i) a gradual rise is followed by a sudden fall or (ii) the pattern is inverted and a sudden rise is followed by a gradual fall. It has been recognized that downdrafts (or sweeps) and updrafts (or ejections) are the primary constitutive motions of such ramp-like patterns in boundary-layer turbulence [65]. However, the difference between the occurrence frequencies of motif "1234" and motif "4321" is much larger under stable conditions than under unstable conditions, as shown in Fig. 3(a), which means the heterogeneity is much heavier for vertical velocity under stable conditions. This heterogeneous property is related to turbulence intermittency and the dominated non-Gaussian behaviors found in the wind velocity records under stable conditions [35,56]. What' more, the occurrence frequencies of typical motifs in vertical velocity time series change greatly with different scale factors, because there are many different physical processes over a broad range of scales in the atmosphere, that force, modify and coexist with the ABL turbulence [2–4].

Furthermore, the scale-dependent motifs in latitude and longitude wind velocity (u and v) and temperature (T) series behave similarly to those in vertical wind velocity w though their absolute amplitudes maybe quite different, and the motif entropy analysis based on only limited ordinal patterns can be a suitable tool for testing the scale dependency of motifs in three-dimensional wind fluctuations.

5. Conclusions

The ordinal pattern analysis method focuses on motifs with the finer scales which are embedded within larger scale ramp-like structures, and can quantify the scale-dependent properties of these motifs. And the defined scale of the ramp-like structures boundaries should be carefully taken these motifs with the finer scales into consideration in order to avoid the discrepancy among various methods which is possibly resulted from differences in the interpretation of the various scales of turbulence variations [8,9,18,28]. Deep understanding can be obtained from studying motif entropy variation with time under different land surface processes. This would enable better understanding of physical properties and spatial-temporal scales of boundary-layer turbulence.

Acknowledgments

References

[1] Belušić D, Mahrt L. Is geometry more universal than physics in atmospheric boundary layer flow? J Geophys Res 2012;117:D09115. doi:10.1029/2011JD016987.
[2] Thomas C, Foken T. Organised motion in a tall spruce canopy: temporal scales, structure spacing and terrain effects. Boundary-Layer Meteorol 2006;122(1):123–47.
[3] Belušić D, Mahrt L. Estimation of length scales from mesoscale networks. Tellus A 2008;60(4):706–15.
[4] Sun J, Lenschow DH, et al. Atmospheric disturbances that generate intermittent turbulence in nocturnal boundary layers. Boundary-Layer Meteorol 2004;110(2):255–79.
[5] Gao W, Shaw RH, K TPU. Observation of organized structure in turbulent flow within and above a forest canopy. Boundary-Layer Meteorol 1989;47(1):349–77.
[6] Kyaw TPU, Brunet Y, et al. On coherent structures in turbulence above and within agricultural plant canopies. Agricultural Forest Meteorol 1992;61(1-2):55–68.
[7] Qiu J, Kyaw TPU, Shaw RH. Pseudo-wavelet analysis of turbulence patterns in three vegetation layers.. Boundary-Layer Meteorol 1995;72(1):177–204.
[8] Shapland TM, McElrone AJ, et al. Structure function analysis of two-scale scalar ramps. Part I: theory and modelling. Boundary-Layer Meteorol 2012;145(1):5–25.
[9] Shapland TM, McElrone AJ, et al. Structure function analysis of two-scale scalar ramps. Part II: ramp characteristics and surface renewal flux estimation. Boundary-Layer Meteorol 2012;145(1):27–44.
[10] Taylor RJ. Thermal structures in the lowest layers of the atmosphere. Aus J Phys 1958;11(2):168–76.
[11] Antonia RA, Rajagopalan S, Chambers AJ. Conditional sampling of turbulence in the atmospheric surface layer. J Appl Meteorol 1983;22(1):69–78.
[12] Schols JLJ. The detection and measurement of turbulent structures in the atmospheric surface layer. Boundary-Layer Meteorol 1984;29(1):39–58.
[13] Blackwelder R, Kaplan R. On the wall structure of the turbulent boundary layer. J Fluid Mech 1976;76(1):89–112.
[14] Segalini A, Alfredsson PH. Techniques for the eduction of coherent structures from flow measurements in the atmospheric boundary layer. Boundary-Layer Meteorol 2012;143(3):433–50.
[15] Gao W, Shaw RH, Paw KTU. Conditional analysis of temperature and humidity microfronts and ejection/sweep motions within and above a deciduous forest. Boundary-Layer Meteorol 1992;59(1):35–57.
[16] Boppe RS, Neu WL, Shuai H. Large-scale motions in the marine atmospheric surface layer. Boundary-Layer Meteorol 1999;92(2):165–83.
[17] Oikawa S, Meng Y. Turbulence characteristics and organized motion in a suburban roughness sublayer. Boundary-Layer Meteorol 1995;74(3):289–312.
[18] Collineau S, Brunet Y. Detection of turbulent coherent motions in a forest canopy part II: Time-scales and conditional averages. Boundary-Layer Meteorol 1993;66(1-2):49–73.
[19] Hagelberg CR, Gamage NKK. Structure-preserving wavelet decompositions of intermittent turbulence. Boundary-Layer Meteorol 1994;70(3):217–46.
[20] Chen J, Hu F. Coherent structures detected in atmospheric boundary-layer turbulence using wavelet transforms at Huaihe river basin, China. Boundary-Layer Meteorol 2003;107(2):429–44.
[21] Collineau S, Brunet Y. Detection of turbulent coherent motions in a forest canopy part I: Wavelet analysis. Boundary-Layer Meteorol 1993;65(4):357–79.
[22] Horiguchi M, Hayashi T, et al. Observations of coherent turbulence structures in the near-neutral atmospheric boundary layer. Boundary-Layer Meteorol 2010;136(1):25–44.
[23] Barthlott C, Drobinski P, et al. Long-term study of coherent structures in the atmospheric surface layer. Boundary-Layer Meteorol 2007;125(1):1–24.
[24] Chen W, Novak MD, et al. Coherent eddies and temperature structure functions for three contrasting surfaces. Part I: Ramp model with finite microfront time. Boundary-Layer Meteorol 1997;84(1):99–124.
[25] Van Atta C. Effect of coherent structures on structure functions of temperature in the atmospheric boundary layer. Archiwum Mechaniki 1977;29(1):161–71.
[26] Frisch U. Turbulence: the legacy of A. N. Kolmogorov. Cambridge: Cambridge University Press; 1995.
[27] Calif R, Schmitt FG. Multiscaling and joint multiscaling description of the atmospheric wind speed and the aggregate power output from a wind farm. Nonlinear Process Geophys 2014;21(2):379–92.
[28] Yuan YM, Mokhtarzadeh-Dehghan MR. A comparison study of conditional-sampling methods used to detect coherent structures in turbulent boundary layers. Phys Fluids 1994;6(6):2038–57.
[29] Bandt C, Pompe B. Permutation entropy: a natural complexity measure for time series. Phys Rev Lett 2002;88(17):174102.
[30] Graff G, Graff B, et al. Ordinal pattern statistics for the assessment of heart rate variability. Eur Phys J Special Topics 2013;222(2):525–34.
[31] Barreiro M, Marti AC, Masoller C. Inferring long memory processes in the climate network via ordinal pattern analysis. Chaos 2011;21(1):013101.
[32] Tirabassi G, Masoller C. Unravelling the community structure of the climate system by using lags and symbolic time-series analysis. Sci Reports 2016;6:29804.
[33] Aragoneses A, Rubido N, et al. CORRIGENDUM: distinguishing signatures of determinism and stochasticity in spiking complex systems. Sci Reports 2014;3(19):1778.
[34] Aragoneses A, Perrone S, et al. Unveiling the complex organization of recurrent patterns in spiking dynamical systems. Sci Reports 2014;4(8):4696.
[35] Li QL, Fu ZT. Permutation entropy and statistical complexity quantifier of nonstationarity effect in the vertical velocity records. Phys Rev E 2014;89(1):012905.
[36] Li C-T, Hwang M-S, Chu Y-P. A secure and efficient communication scheme with authenticated key establishment and privacy preserving for vehicular ad hoc networks. Comput Commun 2008;31(12):2803–14.
[37] Memon I. Authenticated privacy preserving for continuous query in location based services. J Comput Inf Syst 2013;9(24):9857–64.
[38] Memon I, Ali Q, Zubedi A, Mangi FA. DPMM: dynamic pseudonym-based multiple mix-zones generation for mobile traveler. Multimedia Tools & Applications; 2016. p. 1–30. doi:10.1007/s11042-016-4154-z.
[39] Memon I, Arain QA, Memon MH, et al. Search me if you can: multiple mix zones with location privacy protection for mapping services. Int J Commun Syst 2017. https://doi.org/10.1002/dac.3312.
[40] Memon I, Chen L, Majid A, et al. Travel recommendation using geo-tagged photos in social media for tourist. Wireless Person Commun 2015;80(4):1347–62.
[41] Arain QA, Memon H, Memon I, et al. Intelligent travel information platform based on location base services to predict user travel behavior from user-generated GPS traces. Int J Comput Appl 2017;39(3):155–68.
[42] Akhtar R, Leng S, Memon I, Ali M, Zhang L. Architecture of hybrid mobile social networks for efficient content delivery. Wireless Person Commun 2015;80(1):85–96.
[43] Arain QA, Memon I, Deng Z, et al.. Location monitoring approach: multiple mix-zones with location privacy protection based on traffic flow over road networks, 3. Multimedia Tools & Applications; 2017. p. 1–45.
[44] Memon MH, Khan A, Li JP, et al. Content based image retrieval based on geo-location driven image tagging on the social web. In: International computer conference on wavelet active media technology and information processing; 2015. p. 280–3.

[45] Memon MH, Li J-P, Memon I, Arain QA. GEO matching regions: multiple regions of interests using content based image retrieval based on relative locations. Multimed. Tools Appl 2016;76(14):15377–411.

[46] Memon MH, Li JP, Memon I, et al. Efficient object identification and multiple regions of interest using CBIR based on relative locations and matching regions. In: International computer conference on wavelet active media technology and information processing; 2016. p. 247–50.

[47] Valipour M. Number of required observation data for rainfall forecasting according to the climate conditions. Am J Sci Res 2012;74:79–86.

[48] Valipour M, Montazar AA. An evaluation of SWDC and WinSRFR models to optimize of infiltration parameters in furrow irrigation. Am J Sci Res 2012;69:128–42.

[49] Valipour M. Increasing irrigation efficiency by management strategies: cutback and surge irrigation. J Agricultural Bio Sci 2013;8(1):35–43.

[50] Valipour M. Application of new mass transfer formulae for computation of evapotranspiration. J Appl Water Eng Res 2014;2(1):33–46.

[51] Valipour M. Study of different climatic conditions to assess the role of solar radiation in reference crop evapotranspiration equations. Arch Agron Soil Sci 2015;61(5):679–94.

[52] Valipour M, Sefidkouhi MAG, Raeini–Sarjaz M. Selecting the best model to estimate potential evapotranspiration with respect to climate change and magnitudes of extreme events. Agricultural Water Manag 2017;1(80):50–60.

[53] Chen H, Chen J, et al. The coherent structure of water vapour transfer in the unstable atmospheric surface layer. Boundary-Layer Meteorol 2004;111(3):543–52.

[54] Li X, Hu F, Liu G. Characteristics of chaotic attractors in atmospheric boundary-layer turbulence. Boundary-Layer Meteorol 2001;99(2):335–45.

[55] Wang J, Fu Z, et al. Information entropy analysis on turbulent temperature series in the atmospheric boundary-layer. Plateau Meteorol 2005;24(1):38–42.

[56] Fu ZT, Li QL, et al. Multi-scale entropy analysis of vertical wind variation series in atmospheric boundary-layer. Commun Nonlinear Sci Numer Simul 2014;19(1):83–91.

[57] Wesson K, Katul G, Siqueira M. Quantifying organization of atmospheric turbulent eddy motion using nonlinear time series analysis. Boundary-Layer Meteorol 2003;106(3):507–25.

[58] Antonia RA, Chambers AJ, et al. Temperature ramps in the atmospheric surface layer. J Atmos Sci 1978;36(36):99–108.

[59] Krusche N, Oliveira APD. Characterization of coherent structures in the atmospheric surface layer. Boundary-Layer Meteorol 2004;110(2):191–211.

[60] Bandt C, Pompe B. Permutation entropy: a natural complexity measure for time series. Phys Rev Lett 2002;88(17):174102.

[61] Zunino L, Olivares F, Scholkmann F, Rosso OA. Permutation entropy based time series analysis: equalities in the input signal can lead to false conclusions. Phys Lett A 2017;381(22):1883–92.

[62] Zunino L, Soriano MC, Rosso OA. Distinguishing chaotic and stochastic dynamics from time series by using a multiscale symbolic approach. Phys Rev E 2012;86:046210.

[63] Olivares F, Zunino L, Rosso OA. Quantifying long-range correlations with a multiscale ordinal pattern approach. Physica A 2016;445:283–94.

[64] Ribeiro HV, Zunino L, et al. Complexity–entropy causality plane: A useful approach for distinguishing songs. Physica A 2012;391(7):2421–8.

[65] Katul G, Kuhn G, et al. The ejection-sweep character of scalar fluxes in the unstable surface layer. Boundary-Layer Meteorol 1997;83(1):1–26.

[66] Soriano MC, Zunino L, et al. Time scales of a chaotic semiconductor laser with optical feedback under the lens of a permutation information analysis. IEEE J Quant Electron 2011;47(2):252–61.

[67] Zunino L, Soriano MC, et al. Permutation-information-theory approach to unveil delay dynamics from time-series analysis. Phys Rev E 2010;82(4):046212.

[68] Kavasseri RG, Nagarajan R. Evidence of crossover phenomena in wind-speed data. Circuits Syst I Regular Papers IEEE Trans 2004;51(11):2255–62.

[69] Mahrt L. Intermittency of atmospheric turbulence. J Atmos Sci 1989;46(1):79–95.

[70] Peinke J, Barth S, et al. Turbulence, a challenging problem for wind energy. Physica A 2004;338(1–2):187–93.

[71] She ZS, Fu ZT, et al. Hierarchical structures in climate and atmospheric turbulence. Progress Nat Sci 2002;12(10):747–52.

[72] Boettcher F, Renner CH, et al. On the statistics of wind gusts. Boundary-Layer Meteorol 2003;108(1):163–73.

[73] Liu L, Hu F, et al. Probability density functions of velocity increments in the atmospheric boundary layer. Boundary-Layer Meteorol 2010;134(2):243–55.

[74] Liu L, Hu F, Cheng XL. Probability density functions of turbulent velocity and temperature fluctuations in the unstable atmospheric surface layer. J Geophys Res 2011;116(D12):1248–56.